Arch Virol (1995) 140: 2107–2122

Archives of Virology



# Ultrastructural characteristics of Sin Nombre virus, causative agent of hantavirus pulmonary syndrome

**C. S. Goldsmith, L. H. Elliott, C. J. Peters,** and **S. R. Zaki**

Division of Viral and Rickettsial Diseases, National Center for Infectious Diseases, Centers for Disease Control and Prevention, Atlanta, Georgia, U.S.A.

Accepted August 20, 1995

**Summary.** A previously unrecognized disease, hantavirus pulmonary syndrome, was described following an outbreak of severe, often lethal, pulmonary illness in the southwestern United States in May–June, 1993. We have now studied the morphologic features of the causative agent, Sin Nombre virus (SNV), by thin section electron microscopy and immunoelectron microscopy of infected Vero E6 cells. SNV virions were roughly spherical and had a mean diameter of 112 nm. They had a rather dense envelope and closely apposed fine surface projections, 7 nm in length. Filamentous nucleocapsids were present within virions. Viral inclusion bodies were present in the cytoplasm of infected cells; these appeared granular or filamentous, depending on the plane of section. All of these characteristics were similar to published descriptions of other hantaviruses; however, unlike all other hantaviruses and virtually all other member viruses of the family *Bunyaviridae* which bud upon smooth intracytoplasmic membranes, SNV budding occurred almost entirely upon the plasma membrane of infected cells. Virus budding was associated with the formation of long 28 nm diameter tubular projections. Occasional elongated 47 nm diameter virus-like particles were seen to bud upon intracytoplasmic membranes. As shown by immunoelectron microscopy, viral antigens were localized over virions, inclusions, and tubular projections associated with virion morphogenesis.

## Introduction

In May 1993, a cluster of fatalities due to respiratory failure occurred in the southwestern United States, in an area known as the Four Corners region. The patients developed an influenza-like illness, which rapidly progressed to pulmonary edema and respiratory insufficiency [4]. The cause of the disease, now known as hantavirus pulmonary syndrome (HPS), was quickly identified as a previously unrecognized hantavirus by using a combination of serologic, molecular, and immunohistochemical approaches [14, 20, 35]. The causative agent, Sin Nombre

virus (SNV), was isolated from a deer mouse, *Peromyscus maniculatus*, the natural reservoir and vector of this zoonotic virus [6, 9, 11, 27].

SNV is closely related to other viruses in the genus *Hantavirus*, family *Bunyaviridae*. The family *Bunyaviridae* was segregated from the large arbovirus group in 1975 on the basis of serologic, ultrastructural, and later, molecular characteristics [3, 10, 19, 23]. The family has been divided into five genera [28]: *Bunyavirus* (prototype, Bunyamwera virus), *Hantavirus* (prototype, Hantaan virus), *Nairovirus* (prototype, Nairobi sheep disease virus), *Phlebovirus* (prototype, sandfly fever Sicilian virus), and *Tospovirus* (prototype, tomato spotted wilt virus); several otherwise unassigned viruses have also been placed in the family. The genera of the family *Bunyaviridae* can be differentiated morphologically by negative-stain electron microscopy [15]. Hantaviruses, in particular, show a distinguishing grid-like pattern on the viral envelope. The bunyavirus genome consists of three segments of single-stranded, negative-sense RNA that form helical nucleocapsids by combining with the nucleoprotein [2, 21, 26, 29]. Unlike most negative-sense RNA viruses, the members of the family *Bunyaviridae* have no matrix protein; their nucleocapsids apparently interact directly with the envelope glycoproteins, G1 and G2, during virus formation. Maturation of viral particles occurs upon Golgi or endoplasmic reticulum membranes; in rare exceptions [1, 19] assembly also occurs at the plasma membrane.

This report describes the ultrastructural features of SNV grown in Vero E6 cells. Immunogold labeling was used to further analyze various aspects of the morphogenesis of this newly recognized virus. Comparisons with other hantaviruses and bunyaviruses are also discussed.

## Materials and methods

### *Virus isolation*

The isolation of SNV has been previously described [9]. Briefly, lung tissue from a polymerase chain reaction-positive, seronegative *Peromyscus maniculatus* was inoculated intraperitoneally into laboratory-bred *P. maniculatus* mice. After two passages in these mice, the lung tissue was inoculated into Vero E6 cells, from which an isolate was obtained. All isolation work was performed in a biosafety level 4 laboratory.

### *Electron microscopy*

Infected and uninfected Vero E6 cells were fixed in situ with phosphate-buffered 2.5% glutaraldehyde and immediately scraped from the flasks and pelleted. The cells were then allowed to fix for 2 h while being gamma-irradiated. Next, the cell pellets were postfixed with 1% buffered osmium teroxide, *en bloc* stained with 4% uranyl acetate, dehydrated through a graded series of alcohols and propylene oxide, and embedded in a mixture of Epon-substitute and Araldite [17].

### *Immunogold electron microscopy*

For preembedded immunoelectron microscopy, infected and uninfected Vero E6 cells were fixed in situ with phosphate-buffered 1.5% paraformaldehyde and 0.025% glutaraldehyde,

scraped from the flasks, and allowed to fix in suspension for 2 h. At each of the following immunolabeling steps, cells were pelleted and then resuspended. First, cells were rinsed in phosphate buffer and then resuspended in 1% ovalbumin. Cells were resuspended in a 1:50 dilution of sera from infected or uninfected *P. maniculatus*, or in a 1:100 dilution of the GB04-BF07 monoclonal antibody (MAb), which is directed against the nucleocapsid protein (NP) of Puumala virus [25], a closely related hantavirus. The antibodies were diluted in phosphate buffer with 1% bovine serum albumin (PB/BSA). Cells were rinsed four times with PB/BSA and then resuspended in a secondary goat anti-mouse antibody conjugated to 10 nm colloidal gold particles (Amersham Life Science Inc.; British BioCell International) diluted in PB/BSA with 1% fish gelatin added. Cells were rinsed three times in PB/BSA, rinsed in phosphate buffer, pelleted, and postfixed in glutaraldehyde. The immunogold-labeled cell pellets were then embedded in Epon-substitute/Araldite as described above.

For postembedded immunoelectron microscopy, infected and uninfected Vero E6 cells were fixed in situ with 1.5% paraformaldehyde and 0.025% glutaraldehyde, scraped from the flasks and pelleted, and fixed for 2 h. Cell pellets were dehydrated through a graded series of alcohols, up to 85% alcohol, and embedded in LR White (London Resin Company). Sections were processed for immunolabeling on nickel mesh grids. Dilution and rinse buffers consisted of 0.01 M phosphate-buffered saline, 1% BSA, 0.2% Tween 20, and 0.1% Triton-X. Sections were sequentially placed on drops of 1% ovalbumin and on appropriate dilutions of primary antibody. Antibodies were again from sera of infected or uninfected *P. maniculatus*, and the GB04-BF07 MAb or a control MAb. Sections were rinsed five times and allowed to react with a secondary goat anti-mouse antibody conjugated to 10 nm colloidal gold particles in the diluent with 1% fish gelatin added. Sections were rinsed five times in rinse buffer, then rinsed in $dH_2O$, stained with 1% osmium tetroxide, and rinsed again in $dH_2O$. The sections were stained with uranyl acetate, and some were also stained with lead citrate.

## Results

### *Ultrastructural characterization of Sin Nombre virus*

The morphologic features of the virus particles grown in Vero E6 culture cells were similar to those of other hantaviruses [32] (Fig. 1A, B). Extracellular particles were round to slightly oval, with an average diameter of 112 nm (range: 71 to 149 nm). Only those particles having a distinct osmiophilic membrane were measured. Closely apposed fuzzy surface projections, approximately 7 nm in length, were observed on the viral envelope. The envelope surrounded strands of nucleocapsid that in most particles were arranged in a delicate tangle of filaments showing occasional granularity. In some particles the nucleocapsid formed a more orderly arrangement of parallel filaments or coils (see Fig. 5C). This latter pattern could also be seen in a few elongated, "peanut"-shaped particles (Figs. 1B, 2A).

Virus particles usually appeared as single particles lined up along the plasma membrane (Fig. 2A). Clusters of virus particles were also found close to the surface of infected cells and were often seen at the area of overlap between two cells (Fig. 2B).

On rare occasions, virus-like particles were also found budding into the cisternae of Golgi membranes (Fig. 3). These elongated forms were more narrow than the whole extracellular particles, averaging only 47 nm, and contained distinctive cross-striations. When multiple sections of a single cell were

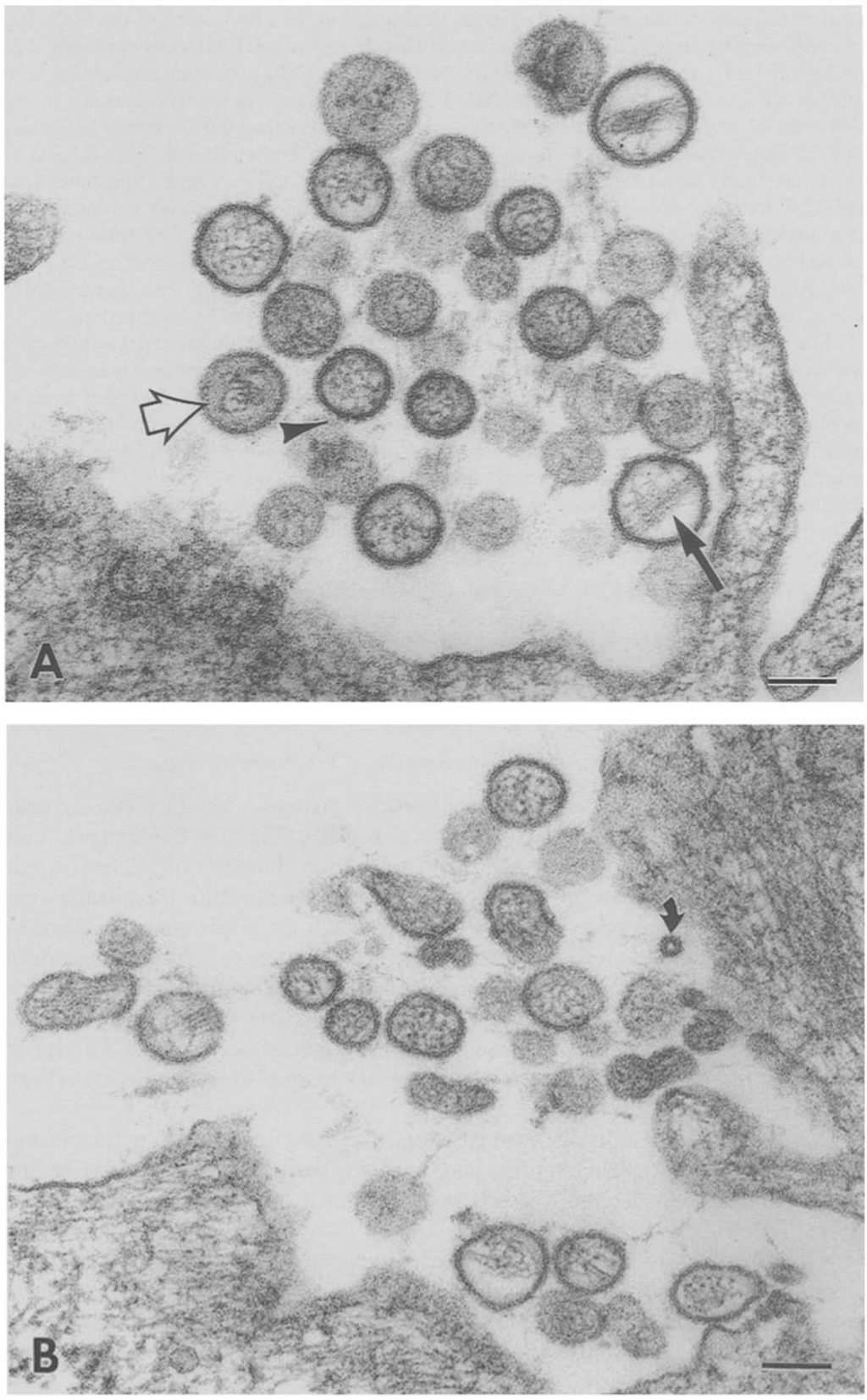
A
B

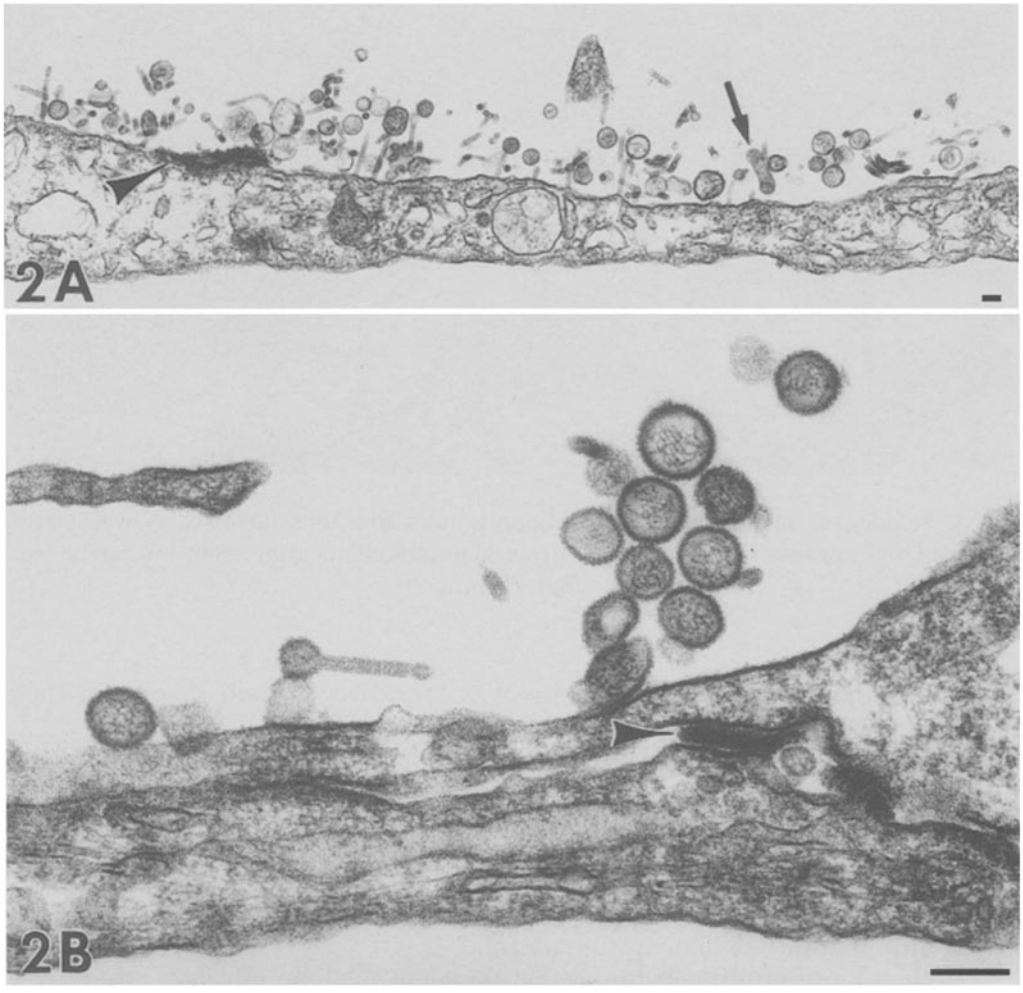


**Fig. 2.** Typical accumulations of extracellular SNV particles. **A** SNV commonly lined up along a long expanse of the cell surface. Also present were rod-shaped tubules and occasionally a dense surface layer (arrowhead). Arrow: Peanut-shaped particle. **B** Virus particles were often found at the junction between two cells. Here, the dense surface layer was compressed between adjoining cells (arrowhead). Bars: 100 nm

**Fig. 1A, B.** Extracellular SNV particles grown in Vero E6 cells. The mostly spherical and occasional "peanut"-shaped particles have fine, closely apposed surface projections and a rather dense envelope (arrowhead). Granulofilamentous nucleocapsids were occasionally arranged in parallel arrays (arrow). Some particles showed a hazy ring beneath the envelope (open arrow). The clusters of extracellular virus particles were sometimes associated with wispy filamentous material of unknown origin, although this material was also seen in the uninfected control cells. Curved arrow: Cross-section of tubular projection. Bars: 100 nm

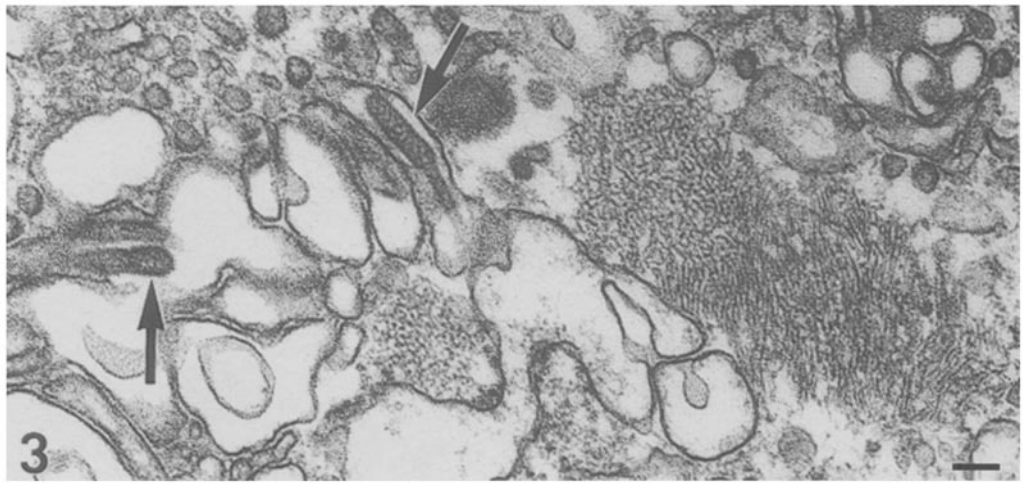


**Fig. 3.** Slender, elongated particles containing cross-striations (arrows) as were rarely observed budding into Golgi cisternae. A typical granulofilamentous inclusion can be seen. Bar: 100 nm

examined, the same Golgi apparatus was found to contain several of these elongated particles budding into the cisternae (Fig. 4A–C).

Several other structures were associated with SNV-infected cells. Tubular projections extended from the cell surface and were sometimes associated with virus particles (Fig. 5A–C). In cross-section, these tubules were composed of two concentric rings (see Fig. 1B). They measured up to 550 nm long but were only 28 nm wide, and occasionally expanded out to form spherical blebs, although apparently without nucleocapsid material.

Typical hantaviral inclusions were prevalent in these infected culture cells and were often associated with the Golgi apparatus (Fig. 6A, B). Most inclusions had either a granular or a filamentous form, but some were granulofila- mentous. The granular inclusions were usually round or oval, whereas the filamentous inclusions were more elongated, up to 4.4 μm in length.

Some infected cells had a fuzzy, dense layer along the plasma membrane (Fig. 7). Vesicles were sometimes seen within this material.

### *Immunoelectron microscopy*

Viral antigens were detected on virus particles (Fig. 8A) and on inclusions (Fig. 8B, C) with both the *P. maniculatus* sera and the GB04-BF07 MAb, using postembedded immunogold labeling of sectioned cells. Occasionally, structures found within the Golgi apparatus were labeled.

When preembedded immunogold was used, viral antigens were detected on the surface of virus particles (Fig. 9A) and tubular projections (Fig. 9B) with the *P. maniculatus* sera but not with the GB04-BF07 MAb (Fig. 10A). The latter finding was not surprising because the MAb recognizes hantaviral nucleocapsid

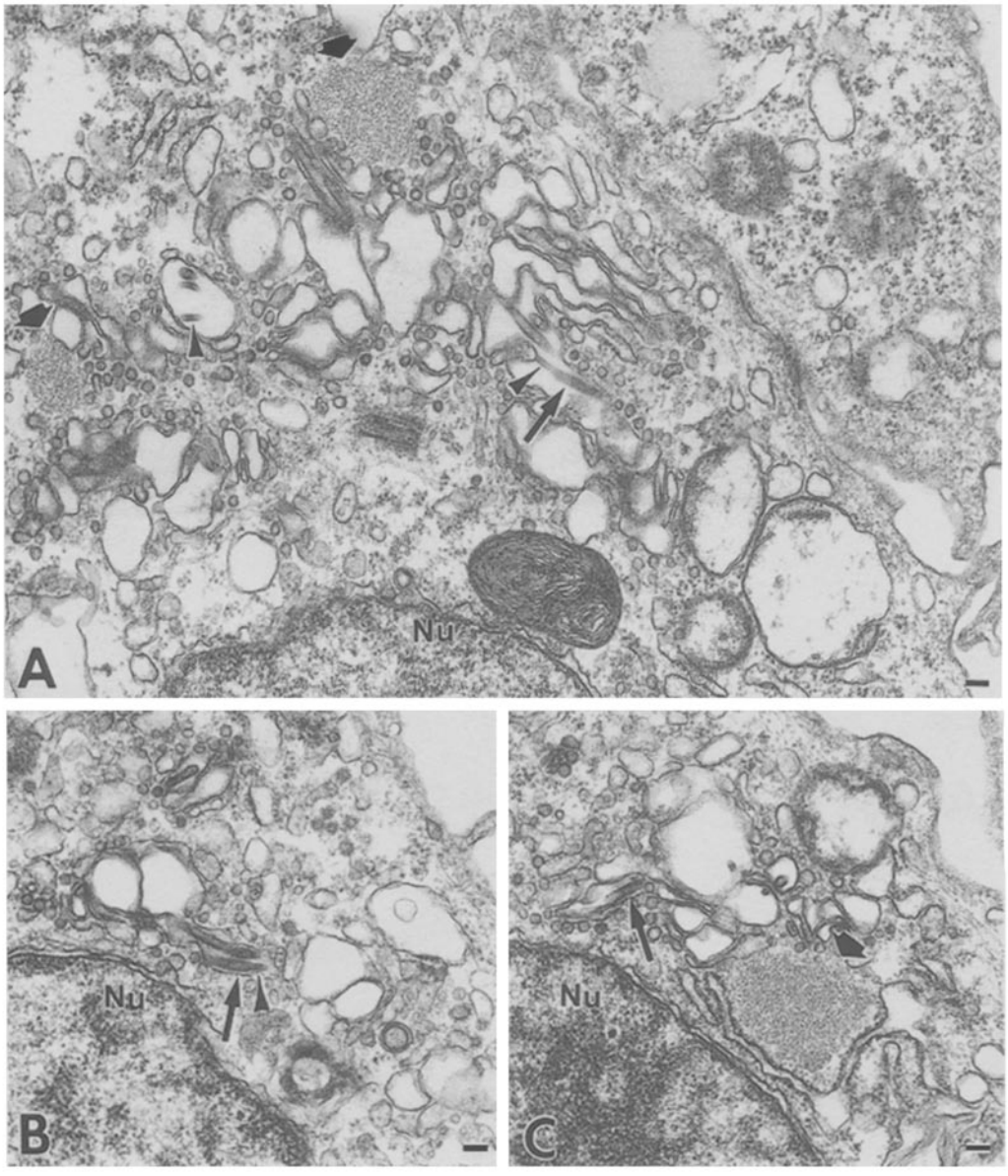


**Fig. 4 A–C.** Semi-serial sections of a cell showing narrow, elongated viral particles (arrows) budding into different regions of the same Golgi complex. Note connection of some particles to Golgi membranes via rod-shaped tubules (arrowheads). *Nu* Nucleus, broad arrows: hantaviral inclusions. Bars: 100 nm

proteins which are not exposed on the viral surface. This MAb did show a small amount of immunogold labeling of debris associated with some particles, but this material appeared to be derived from inclusions from lysed cells. No specific labeling of the dense surface layer was seen by using either pre- or postembedded immunolabeling (Fig. 10B).

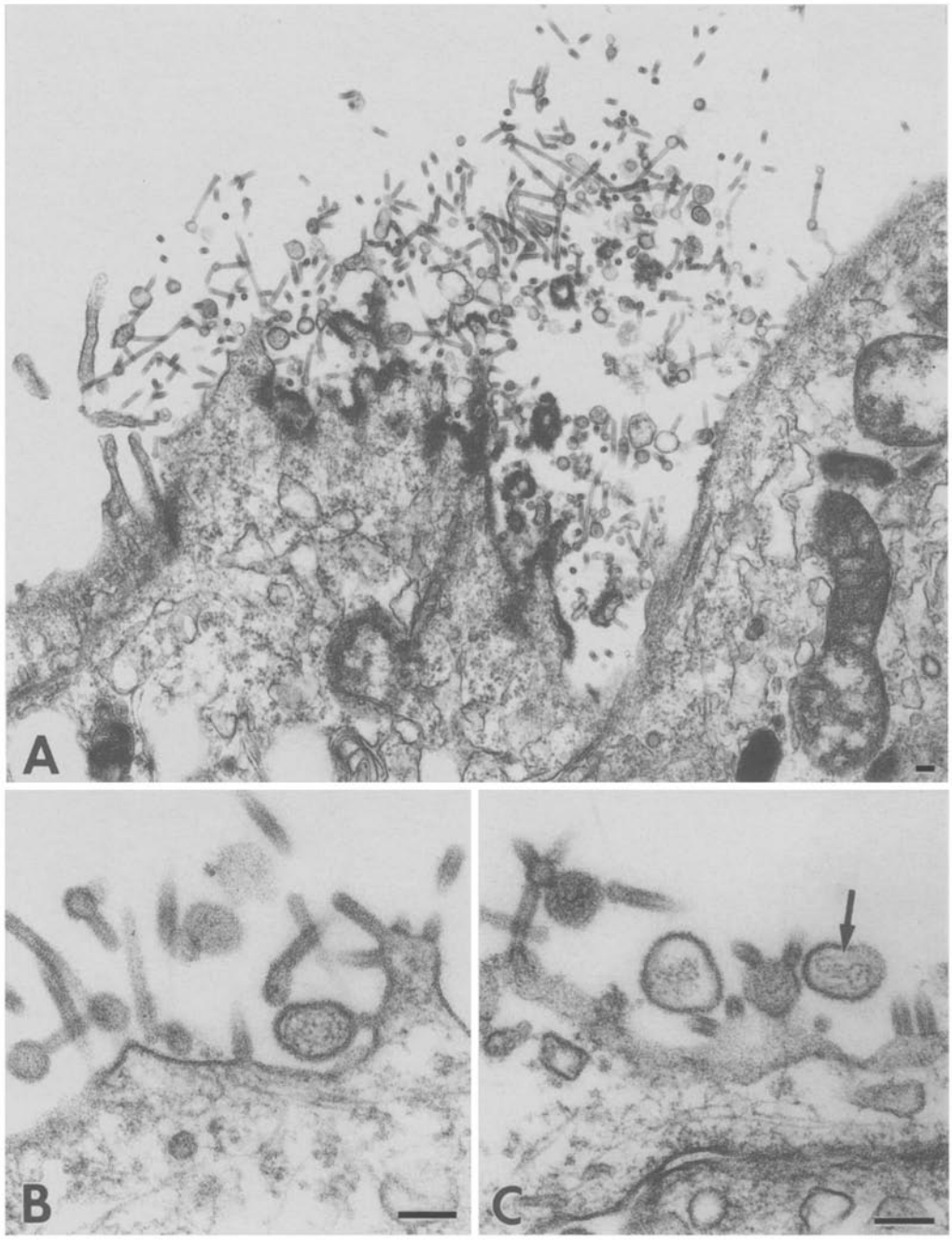


**Fig. 5.** Tubular projections along the cell surface of SNV-infected Vero E6 cells. **A** Large accumulations of the tubules were frequently observed and may represent an overproduction of the viral envelope glycoproteins. **B** SNV particle budding from the cell surface. **C** Rods were often seen attached to whole virus particles. Also present was a particle containing a "coiled" nucleocapsid (arrow). Bars: 100 nm

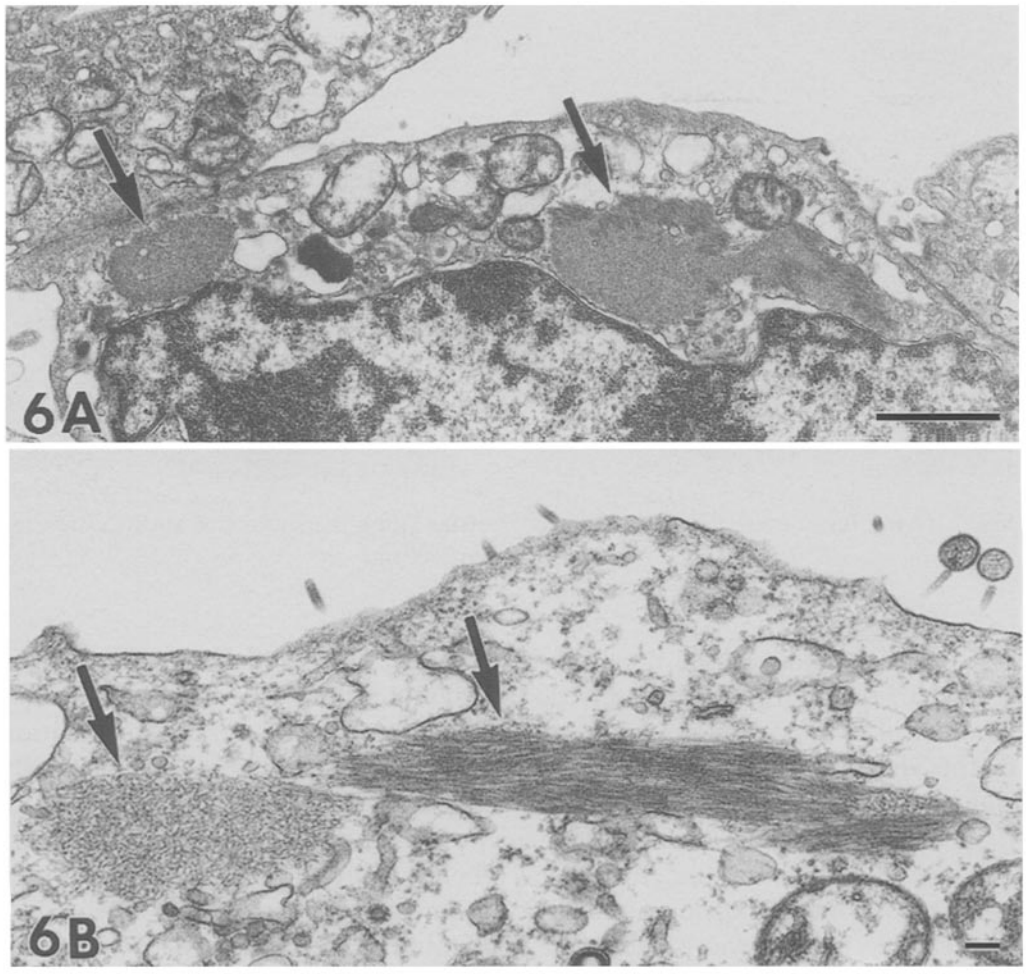


**Fig. 6 A, B.** Typical hantaviral inclusions showing granular and filamentous structures (arrows). Viral inclusions were often closely associated with the Golgi apparatus. Bars: 1 μm (**A**); 100 nm (**B**)

## Discussion

HPS has a high mortality rate, and in a majority of fatal cases death occurs within two days of hospitalization as a result of vascular dysfunction and a capillary leak syndrome [8, 35]. Viral antigens have been identified in microvascular endothelial cells in tissues of HPS cases by using immunohistochemical staining, with the most extensive immunostaining observed in pulmonary endothelial cells [35]. Granulofilamentous structures similar to the SNV inclusions observed in this study were seen within pulmonary endothelial cells. However, additional evidence was needed to establish their identity. The immunogold labeling technique established in the present study allowed us to confirm their viral nature and to identify pulmonary endothelial cells as sites of viral replication in fatal cases of HPS.

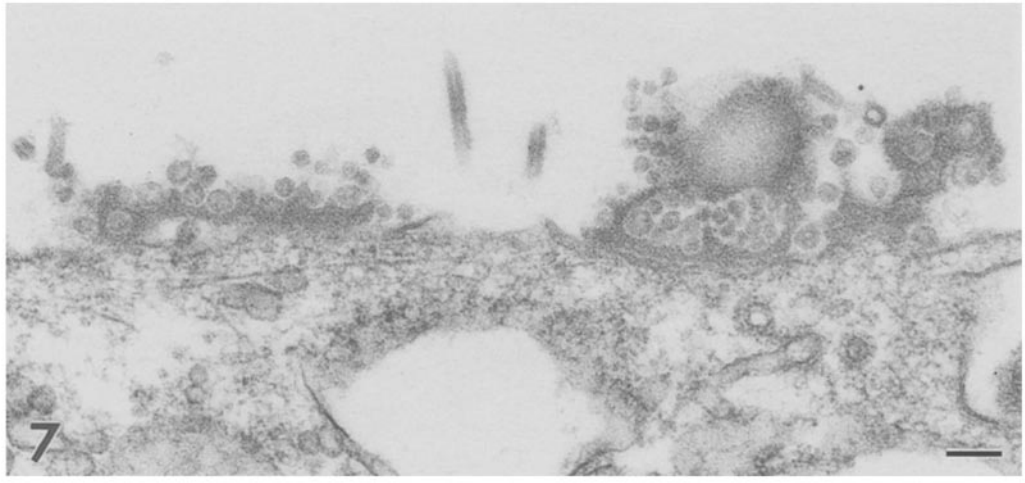


**Fig. 7.** Dense fuzzy material and associated vesicles along the surface of an SNV-infected Vero E6 cell. Bar: 100 nm

Although many of the morphologic features of SNV in Vero E6 cells are similar to those previously described for Hantaan virus [32–34], they are not identical. The most obvious similarity was the filamentous internal organization of the virus particles. In contrast, most of the other members of the family *Bunyaviridae* usually have a more dense and homogenous internal structure [7, 18, 19]. Inclusions were also a conspicuous feature in the cytoplasm of SNV-infected cells, and immunocytochemical labeling showed that the inclusions were composed of nucleocapsid protein. The presence of narrow, elongated virus-like particles has been previously described for Hantaan virus [34] and also for other bunyaviruses [18, 31]. Finally, a dense layer was seen along the surface of SNV-infected cells analogous to that reported for Hantaan virus-infected cells. Tao et al. [34] had suggested the viral nature of this layer on the basis of immunoperoxidase analysis; however, using immunogold labeling, we could not detect specific labeling of this layer.

Two differences between SNV- and Hantaan virus-infected cells are noteworthy. First, tubular projections along the plasma membrane of infected Vero E6 cells were a prominent feature of SNV infection. While tubules have also been reported in Hantaan virus-infected cells [34], they were less common and primarily seen in association with Golgi membranes. Second, in contrast to reported budding of Hantaan virus upon membranes of the endoplasmic reticulum and/or Golgi [12, 32], SNV matured primarily upon the plasma membrane with only occasional budding of slender, elongated particles into the Golgi.

The significance of this site of budding of SNV is unclear, since most bunyaviruses bud upon intracytoplasmic smooth membranes, mostly Golgi membranes [18, 19, 22]. Rift Valley fever virus (RVFV), a bunyavirus in the *Phlebovirus* genus, is known to bud upon both plasma and intracytoplasmic

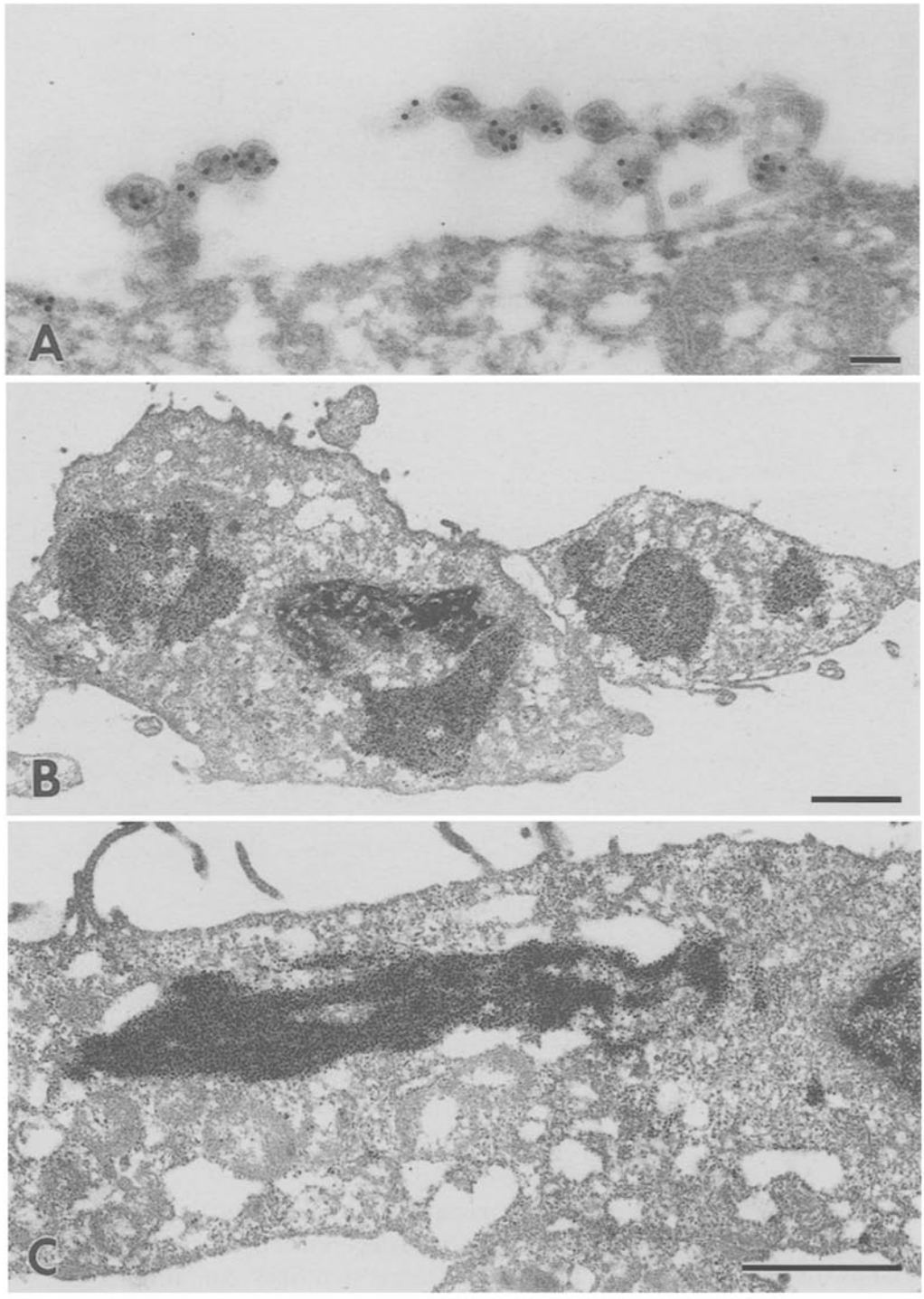


**Fig. 8.** Postembedded immunolocalization of SNV antigens. Nucleoprotein-specific 10 nm-gold label was localized over extracellular viral particles (**A**) and over cytoplasmic inclusions (**B**), by using the GB04-GF07 MAb. **C** Inclusions were also immunogold labeled using the *P. maniculatus* sera. Bars: 100 nm (**A**); 1 μm (**B**, **C**)

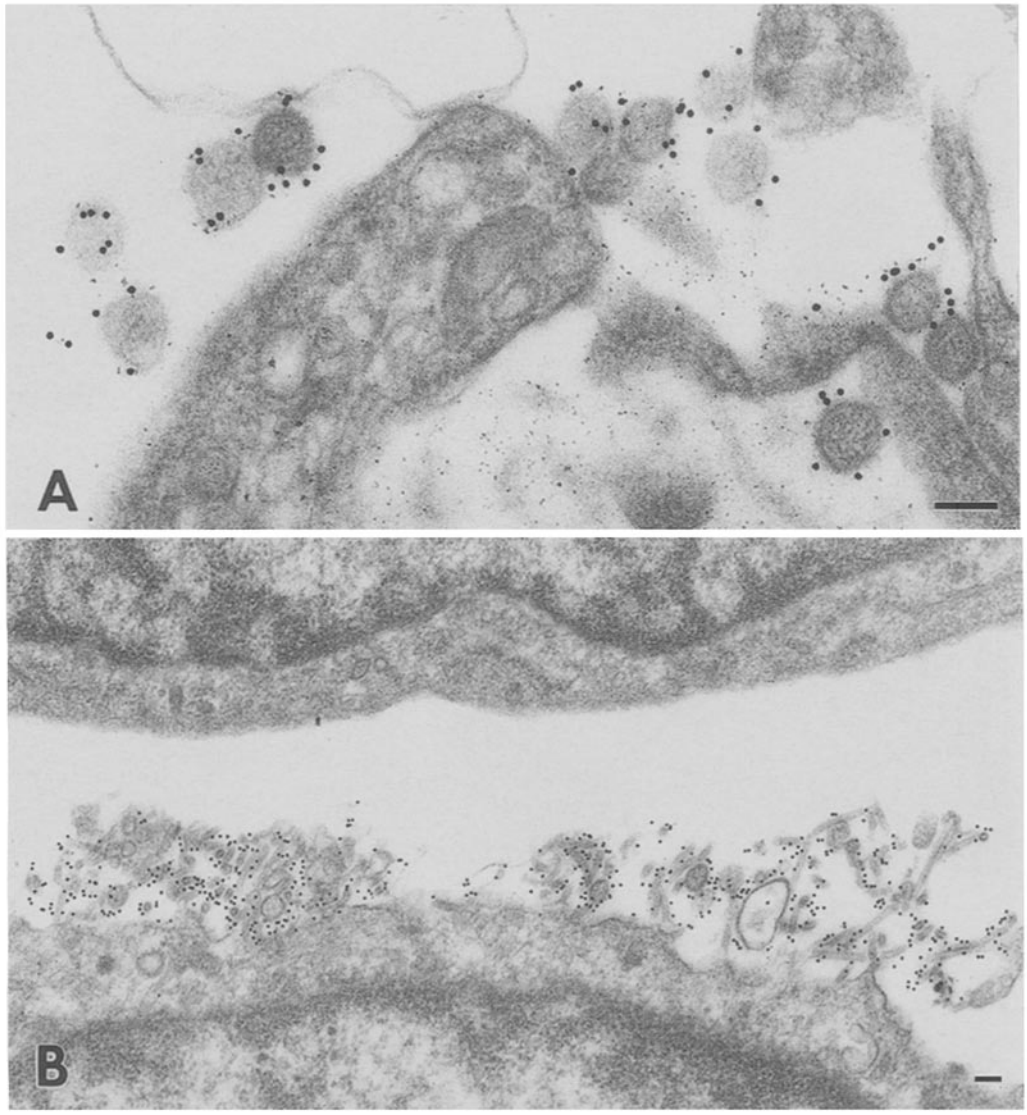


**Fig. 9.** Immunolocalization of SNV-specific surface antigens, using the preembedded labeling technique. Both the whole virus particles (**A**) and tubular projections (**B**) were heavily labeled using the *P. maniculatus* sera. Bars: 100 nm

membranes when grown in primary hepatocyte cell cultures [1]. However, the site of assembly of RVFV was reported to be dependent upon the viral strain as well as the cell culture type used. Of interest is that SNV contains about 23% hydroxylated or sulfhydryl-containing amino acid residues in the transmembrane region of the envelope glycoprotein, G1 [30], a feature which is consistent with a "Golgi retention signal" as was described for Punta Toro virus by Matsuoka et al. [16]. Thus, SNV budding upon the plasma membrane of Vero E6 cells as described raises more questions that require further investigation.

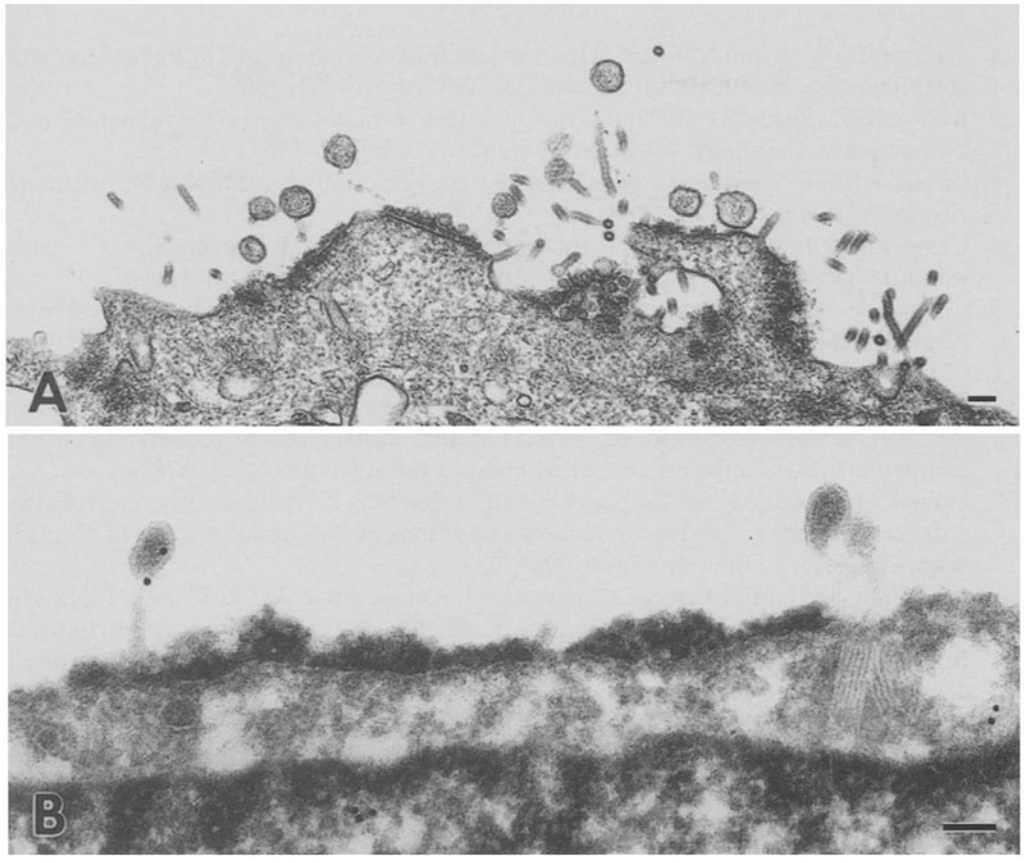


**Fig. 10.** Absence of immunogold labeling in SNV-infected cells. **A** The GB04-GF07 Mab against the nucleocapsid protein of Puumala virus did not specifically label the surface structures using the preembedded method. The dense fuzzy surface layer was not immunogold labeled by either the *P. maniculatus* sera (**B**) or the GB04-GF07 MAb (not shown). Bars: 100 nm

Observations on the morphogenesis of SNV contribute to our understanding of the intricacies of the pathogenesis of HPS. Much remains to be elucidated about SNV infection, including details of viral replication and morphogenesis in the rodent reservoir host, *P. maniculatus*. Other hantaviral variants associated with HPS have recently been identified in the United States [5, 13, 24], and the widening spectrum of associated illnesses and their pathologic features are under investigation.

## Acknowledgements

We are very grateful to Dr. F. A. Murphy for critically reading the manuscript. We thank Jeannette Taylor for embedding the specimens, and John O'Connor for his editorial review.

## References


1. Anderson GW Jr, Smith JF (1987) Immunoelectron microscopy of Rift Valley fever viral morphogenesis in primary rat hepatocytes. Virology 161: 91–100
2. Bishop DHL, Shope RE (1979) *Bunyaviridae*. In: Fraenkel-Conrat HL, Wagner RR (eds) Comprehensive virology, vol 14. Plenum, New York, pp 1–156
3. Casals J (1963) New developments in the classification of arthropod-borne animal viruses. Ann Microbiol 11: 13–34
4. Centers for Disease Control and Prevention (1993) Outbreak of acute illness – southwestern United States, 1993. MMWR Morb Mortal Wkly Rep 42: 421–424
5. Centers for Disease Control and Prevention (1994) Newly identified hantavirus – Florida, 1994. MMWR Morb Mortal Wkly Rep 43: 99–105
6. Childs JE, Ksiazek TG, Spiropoulou CF, Krebs JW, Morzunov S, Maupin GO, Gage KL, Rollin PE, Sarisky J, Enscore RE, Frey J, Peters CJ (1994) Serologic and genetic identification of *Peromyscus maniculatus* as the primary rodent reservoir for a new hantavirus in the southwestern United States. J Infect Dis 169: 1271–1280
7. Donets MA, Chumakov MP, Korolev MB, Rubin SG (1977) Physicochemical characteristics, morphology and morphogenesis of virions of the causative agent of Crimean hemorrhagic fever. Intervirology 8: 294–308
8. Duchin JS, Koster FT, Peters CJ, Simpson GL, Tempest B, Zaki SR, Ksiazek TG, Rollin PE, Nichol S, Umland ET, Moolenaar R, Reef S, Nolte K, Gallagher M, Butler J, Breiman R, Hantavirus Study Group (1994) Hantavirus pulmonary syndrome: a clinical description of 17 patients with a newly recognized disease. N Engl J Med 330: 949–955
9. Elliott LH, Ksiazek TG, Rollin PE, Spiropoulou CF, Morzunov S, Monroe M, Goldsmith CS, Humphrey CD, Zaki SR, Krebs JW, Maupin G, Gage K, Childs JE, Nichol ST, Peters CJ (1994) Isolation of the causative agent of hantavirus pulmonary syndrome. Am J Trop Med Hyg 51: 102–108
10. Fenner F (1975/76) The classification and nomenclature of viruses. Intervirology 6: 1–12
11. Goldsmith CS, Humphrey CD, Elliott LH, Zaki SR (1994) Morphology of Muerto Canyon virus, causative agent of hantavirus pulmonary syndrome. In: Bailey GW, Garratt-Reed AJ (eds) Proceedings of the Microscopy Society of America Fifty-Second Annual Meeting 1994, San Francisco, pp 272–273
12. Hung T, Xia S-M, Zhao TX, Zhou JY, Song G, Liao GXH, Ye WW, Chu YL, Hang CS (1983) Morphological evidence for identfying the viruses of hemorrhagic fever with renal syndrome as candidate members of the *Bunyaviridae* family. Arch Virol 78: 137–144
13. Khan AS, Spiropoulou CF, Morzunov S, Zaki SR, Kohn MA, Nawas SR, McFarland L, Nichol ST (1995) Fatal illness associated with a new hantavirus in Louisiana. J Med Virol 46: 281–286
14. Ksiazek TG, Peters CJ, Rollin PE, Zaki S, Nichol S, Spiropoulou C, Morzunov S, Feldmann H, Sanchez A, Khan AS, Mahy BWJ, Wachsmuth K, Butler J (1995) Identification of a new North American hantavirus that causes acute pulmonary insufficiency. Am J Trop Med Hyg 52: 117–123
15. Martin, ML, Lindsey-Regnery H, Sasso DR, McCormick JB, Palmer E (1985) Distinction between *Bunyaviridae* genera by surface structure and comparison with Hantaan virus using negative stain electron microscopy. Arch Virol 86: 17–28
16. Matsuoka Y, Chen S-Y, Compans RW (1994) A signal for Golgi retention in the bunyavirus G1 glycoprotein. J Biol Chem 269: 22565–22573
17. Mullenhauer HH (1964) Plastic embedding mixtures for use in electron microscopy. Stain Technol 39: 111–114

18. Murphy FA, Harrison AK, Tzianabos T (1968) Electron microscopic observations of mouse brain infected with Bunyamwera group arboviruses. J Virol 2: 1315–1325
19. Murphy FA, Harrison AK, Whitfield SG (1973) *Bunyaviridae*: morphologic and morphogenetic similarities of Bunyamwera serologic supergroup viruses and several other arthropod-borne viruses. Intervirology 1: 297–316
20. Nichol ST, Spiropoulou CF, Morzunov S, Rollin PE, Ksiazek TG, Feldmann H, Sanchez A, Childs J, Zaki S, Peters CJ (1993) Genetic identification of a hantavirus associated with an outbreak of acute respiratory illness. Science 262: 914–917
21. Obijeski JF, Bishop DHL, Palmer E, Murphy FA (1976) Segmented genome and nucleocapsid of La Crosse virus. J Virol 20: 664–675
22. Pettersson RF (1991) Protein localization and virus assembly at intracellular membranes. Curr Top Microbiol Immunol 170: 67–106
23. Pettersson R, Hewlett MJ, Baltimore D, Coffin JM (1977) The genome of Uukuniemi virus consists of three unique RNA segments. Cell 11: 51–63
24. Rollin PE, Ksiazek TG, Elliott LH, Ravkov EV, Martin ML, Morzunov S, Livingstone W, Monroe M, Glass G, Ruo S, Khan AS, Childs JE, Nichol ST, Peters CJ (1995) Isolation of Black Creek Canal virus, a new hantavirus from *Sigmodon hispidus* in Florida. J Med Virol 46: 35–39
25. Ruo SL, Sanchez A, Elliott LH, Brammer LS, McCormick JB, Fisher-Hoch SP (1991) Monoclonal antibodies to three strains of hantaviruses: Hantaan, R22, and Puumala. Arch Virol 119: 1–11
26. Saikku P, von Bonsdorff CH, Brummer-Korvenknotio M, Vaheri A (1971) Isolation of non-cuboidal ribonucleoprotein from Inkoo virus, a Bunyamwera supergroup arbovirus. J Gen Virol 13: 335–337
27. Schmaljohn AL, Li D, Negley DL, Bressler DS, Turell MJ, Korch GW, Ascher MS, Schmaljohn CS (1995) Isolation and initial characterization of a newfound hantavirus from California. Virology 206: 963–972
28. Schmaljohn CS, Beaty BJ, Calisher CH, Dalrymple JM, Elliott RM, Karabatsos N, Kolakofsky K, Lee HW, Lvov DK, Marriott AC, Nuttall PA, Peters D, Pettersson RF, Shope RE (1995) *Bunyaviridae*. In: Murphy FA, Fauquet CM, Bishop DHL, Ghabrial SA, Jarvis AW, Martelli GP, Mayo MA, Summers MD (eds) Virus Taxonomy. Classification and Nomenclature of Viruses. Sixth Report of the International Committee on Taxonomy of Viruses. Springer, Wien New York, pp 300–315 (Arch Virol [Suppl] 10)
29. Schmaljohn CS, Patterson JL (1990) Bunyaviridae and their replication. In: Fields BN, Knipe DM (eds) Fields Virology. Raven Press, New York, pp 1175–1194
30. Spiropoulou CF, Morzunov S, Feldmann H, Sanchez A, Peters CJ, Nichol ST (1994) Genome structure and variability of a virus causing hantavirus pulmonary syndrome. Virology 200: 715–723
31. Stevenson AE, Holmes IH (1972) Electron microscopy of Koongol group arboviruses. Aust J Biol Sci 25: 53–60
32. Tao H (1988) Atlas of hemorrhagic fever with renal syndrome. Science Press, Beijing
33. Tao H, Semao X, Zinyi C, Gan S, Yanagihara R (1987) Morphology and morphogenesis of viruses of hemorrhagic fever with renal syndrome: II. Inclusion bodies – ultrastructural markers of hantavirus-infected cells. Intervirology 27: 45–52
34. Tao H, Zinyi C, Tungxin Z, Semao X, Changshou H (1985) Morphology and morphogenesis of viruses of hemorrhagic fever with renal syndrome (HFRS): I. Some peculiar aspects of the morphogenesis of various strains of HFRS virus. Intervirology 23: 97–108

35. Zaki SR, Greer PW, Coffield LM, Goldsmith CS, Nolte KB, Foucar K, Feddersen RM, Zumwalt RE, Miller GL, Khan AS, Rollin PE, Ksiazek TG, Nichol ST, Mahy BWJ, Peters CJ (1995) Hantavirus pulmonary syndrome: pathogenesis of an emerging infectious disease. Am J Pathol 146: 552–579

Authors' address: C. S. Goldsmith, Mailstop G32, Division of Viral and Rickettsial Diseases, Centers for Disease Control and Prevention, Atlanta, GA 30333, U.S.A.

Received August 7, 1995